

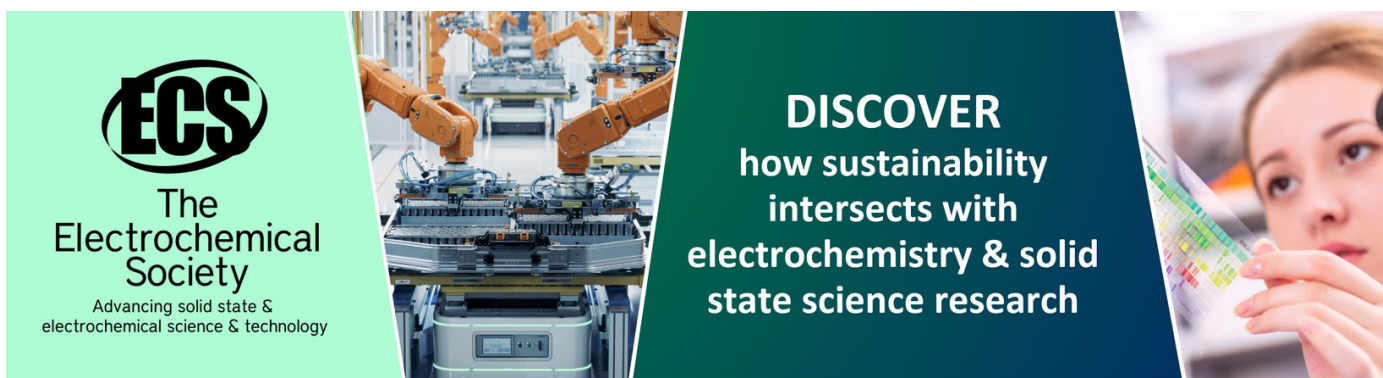
Electro-optic imaging of potential distributions in the quantum Hall regime

To cite this article: R Knott *et al* 1995 *Semicond. Sci. Technol.* **10** 117

View the [article online](#) for updates and enhancements.

You may also like

- [Current distribution and Hall potential landscape towards breakdown of the quantum Hall effect: a scanning force microscopy investigation](#)
K Panos, R R Gerhardt, J Weis et al.
- [Surface Hall Potentiometry for Characterizing Semiconductor Films](#)
Kenta Arima, Kenji Hiwa, Ryoji Nakaoka et al.
- [A four-terminal-pair Josephson impedance bridge combined with a graphene-quantized Hall resistance](#)
S Bauer, R Behr, R E Elmquist et al.



ECS
The
Electrochemical
Society
Advancing solid state &
electrochemical science & technology

DISCOVER
how sustainability
intersects with
electrochemistry & solid
state science research

Electro-optic imaging of potential distributions in the quantum Hall regime

R Knott, W Dietsche, K von Klitzing, K Eberl and K Ploog†

Max-Planck-Institut für Festkörperforschung, Postfach 800665, 70506 Stuttgart, Germany

Received 30 August 1994, accepted for publication 10 October 1994

Abstract. The potential distribution in Hall effect experiments on two-dimensional electron systems (2DES) is imaged with a scanning polarization optical microscope utilizing the internal electro-optic effect. Outside the quantum Hall regime (QHR), Hall potential profiles vary linearly between the two edges. In the QHR, the observed Hall potential profile is nonlinear. Its shape depends on magnetic field and current, indicating inhomogeneous current transport in the interior of the 2DES. In the plateau centre, the Hall potential drop is concentrated in the middle of the channel. The results are interpreted in terms of electron density inhomogeneities. These lead to the observed potential distributions because of the very strong dependence of the conductivity on the local electron density.

1. Potentials in two-dimensional magnetotransport

Two-dimensional electron systems (2DES) in semiconductors exposed to a strong perpendicular magnetic field exhibit a remarkable change in their electronic properties. When a small integral number n of electrons is approximately sharing a flux quantum, the Hall resistance of the 2DES is quantized as h/ne^2 . Simultaneously, the dissipative resistance drops to unmeasurably low values. Usually, these global magnetotransport properties of the 2DES have been studied by alloying contacts at the boundaries to feed currents and sense voltages.

A more detailed description of the system, however, demands a finer graining. Interest turns to the local quantities of potential and current in particular. This became clear quite early on [1]. The potential and current distributions in the interior are unfortunately difficult to measure by contacts alloyed in the inside of the 2DES [2]. As well as possibly changing these distributions by their own presence, they may act also as carrier reservoirs. In addition, a necessarily small number of contacts can only yield a coarse picture of the full potential distribution.

Nevertheless, only local measurements can unambiguously elucidate physical situations like the edge channel transport regime at low currents [3] or the breakdown of the quantum Hall effect (QHE) occurring at large transport currents [4]. In these phenomena, inhomogeneous distributions of current and potential should

play a central role [5, 6]. Recently, a mesoscopic self-structure of the 2DES consisting of alternating compressible and incompressible stripes has aroused great interest. These, or externally imposed density inhomogeneities, may cause considerable lateral potential and current variations. Consequently, contactless measurements are desirable to provide a real 2D mapping of the potential distributions in the 2DES and to get clues on these mechanisms.

The linear electro-optic effect (Pockels effect) in III–V compound semiconductors makes contactless potential measurements possible even at liquid-helium temperatures and in high magnetic fields. An electric field applied to the crystal causes birefringence, which changes the ellipticity of subbandgap light passed through the sample [7]. In the last decade this effect has been widely utilized, especially in studies of ultrafast processes in semiconductors [8]. Recently, it has been applied to study the Hall potential profile in a modulation-doped heterostructure subjected to a quantizing magnetic field [9]. In the quantum Hall regime (QHR) around filling factor 4, the profile was found to be significantly nonlinear, with the major potential drop split symmetrically within approximately 150 μm of the system boundaries. This pattern was insensitive to the magnetic field in the Hall plateau region. Outside the QHR, the profile was close to linear.

The pattern of [9] agreed qualitatively with an early theoretical model except that the drop should be over a much shorter length scale [10]. This agreement is surprising because in this model a vanishing conductivity everywhere in the sample is assumed. In the case of a homogeneous but non-zero conductivity a linear profile was predicted, however [11]. In a realistic 2DES sample

† Present address: Paul-Drude-Institut für Festkörperelektronik, Hausvogteiplatz 5-7, 10117 Berlin, Germany.

the conductivity varies laterally because of its strong dependence on carrier concentrations in the QHR. For such cases the main potential drop was expected to occur in the interior of the 2DES. Clearly, further experimental studies are necessary.

In this paper we report imaging experiments based on the electro-optic technique. In these measurements the macroscopic lateral electric potential distributions built up by a transport current in a magnetically quantized 2DES were mapped. The dependence on current and magnetic field in the QHR has been studied in detail. Linear potential drops have been found in a low-mobility sample under all conditions; in a high-mobility sample, however, linear potentials drop occur only outside the QHR. In the QHR step-like potential drops in the interior of the sample are observed.

One should keep in mind that in the electro-optic measurements the electrostatic potential is probed. Thus, there might be differences from the results of galvanically coupled measurements where the electrochemical potential is probed. Locally, an electrochemical potential change may for convenience (but not rigorously) be decomposed into a 'chemical' part due to a density change and an 'electrostatic' part which is set up by the space charge. In our experiments the potential distributions observed electro-optically are closely related with the galvanic measurements which we have done simultaneously, suggesting that changes in the 'chemical' part are negligible. The same conclusion has already been reached in the earlier electro-optical experiment [9].

In section 2 the experimental technique will be described; it is demonstrated by measuring the potential landscape in a low-mobility sample. Section 3 contains results on a high-mobility sample where quantum effects are more pronounced. It is split into subsections on line profiles of the potential (section 3.1), on the images of the potentials inside the sample (section 3.2), on the nonlinear response of the dependence of the potential profile on current (section 3.3) and on the observation of 'non-local' current transport (section 3.4). In section 4 the behaviour of the high-mobility sample is discussed in subsections on the linear (section 4.1) and nonlinear response (section 4.2) as well as on the breakdown and non-local transport behaviour (section 4.3).

2. Experimental details

In these electro-optic experiments circularly polarized light is transmitted through the sample. The two linear components of this light beam experience different phase changes in dependence on the potential difference between the two surfaces of the sample. This causes an elliptic polarization of the transmitted light which is analysed. This technique allows a TV-type imaging of the sample as is demonstrated in [12].

At low temperatures problems with both persistent and non-persistent parallel conduction arose making the TV-type technique impossible because of the necessary

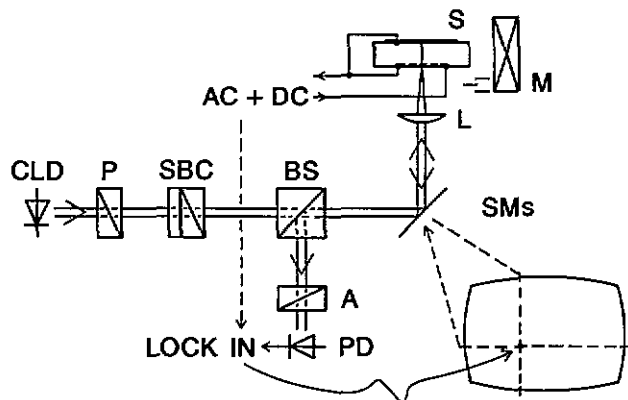


Figure 1. Schematic diagram of the low-temperature set-up. Subbandgap light from the collimated laser diode (CLD) (850 nm, 2 mW) is circularly polarized by the calcite polarizer (P) and the quartz compensator (SBC). Computer-controlled swivelling mirrors (SMs) allow for raster scanning of the focus of lens (L) over the sample (S) inside the magnet (M). Light reflected from the Au-coated back surface of the sample is separated from the incident beam by the beam splitter (BS) and analysed with the calcite prism (A). The photocurrent detected by the Si photodiode (PD) is demodulated in phase with the transport current modulation (AC) by a lock-in amplifier. The result is displayed colour coded on the computer screen.

parallel illumination. Modulation-doped heterostructures are particularly likely to develop a persistent by-pass channel in the doped AlGaAs layer upon illumination. This by-pass may (i) shorten the 2D channel via the alloyed contacts smearing out magnetotransport traces, it may (ii) act as a close gate electrode, and (iii) it may screen the potential distribution in the 2DES towards the sample surface. To circumvent these problems, samples without persistent by-pass must be selected. Non-persistent by-pass effects may arise upon homogeneous illumination of the sample. They were minimized by a laser scanning technique where only one point of the sample is illuminated at a time. Thus, the TV imaging technique could not be used at liquid-helium temperatures.

Consequently, we attached a scanning polarization microscope to an optical cryostat (figure 1) [12]. External galvanometer scanners (SMs) allow for raster scanning of a laser focus over the sample (S) placed in the bore of a superconducting magnet (M). A cryogenic lens (L) yields a fine focus ($\approx 10 \mu\text{m}$). As a source we choose a collimated laser diode (CLD, 850 nm, 2 mW) emitting many longitudinal modes. This light is circularly polarized with a calcite polarizing prism (P) and an appropriately set Soleil-Babinet compensator (SBC).

In the scanning experiments we operate in a reflecting probe geometry, where we analyse the light reflected from the gold-coated, polished back side ((001) surface) of the sample. The analyser (A) converts the polarization changes to intensity changes. These changes are proportional to the potential difference between the sample surface and the backside reference electrode [13]. They are synchronously detected by the Si photodiode

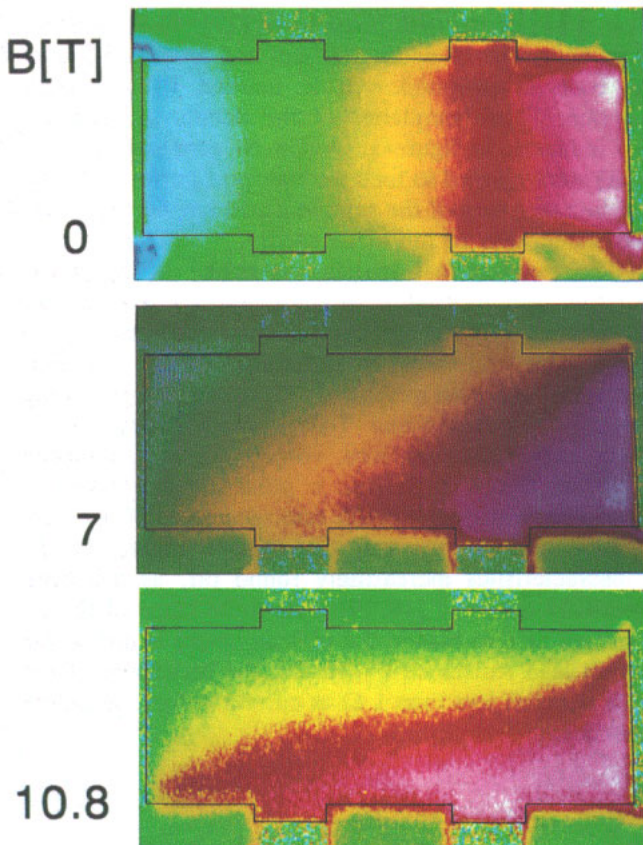


Figure 2. Electro-optically measured potential distributions caused by a current in a delta-doping layer at three magnetic fields ($B = 7 \text{ T} \approx 1/\mu$; $B = 10.8 \text{ T}$ is the centre of the QHE plateau). The boundaries of the 2DES with dimensions $0.5 \times 1.5 \text{ mm}^2$ are indicated by the black lines. The measured potential at each point is colour coded. It increases from blue through green, yellow, red and violet to white.

(PD) and a lock-in amplifier. The laser focus is raster-scanned across the sample under computer control, and the potential signal measured at each point is displayed, brightness or colour-coded at corresponding positions on the computer screen, yielding an image. The potential resolution ($1 \text{ mV Hz}^{-1/2}$ at $10 \mu\text{A}$ photocurrent) is limited by shot noise only.

With this method, we have investigated the potential distributions in delta-doping layers in GaAs [14]. These structures do not show undesired persistent by-pass effects due to their single minimum vertical band structure. Despite their low mobility ($\mu \approx 1.5 \times 10^3 \text{ cm}^2 \text{ V}^{-1} \text{ s}^{-1}$), they exhibited quantized Hall resistance around filling factor 2 [15]. Simultaneously, the longitudinal resistance drops to $\approx 500 \Omega$ at $T = 1.6 \text{ K}$. We have obtained the potential distributions from zero to quantizing magnetic field (figure 2). The tilting of the equipotentials with increasing magnetic field is obvious from the figure. In the case of the QHR (bottom panel) a Hall angle of approximately 90° is realized. In a magnetic field, the potential drops linearly across the sample. The electro-optic potential patterns agree with the galvanically measured electrochemical potentials. This also holds in the non-ohmic transport regime,

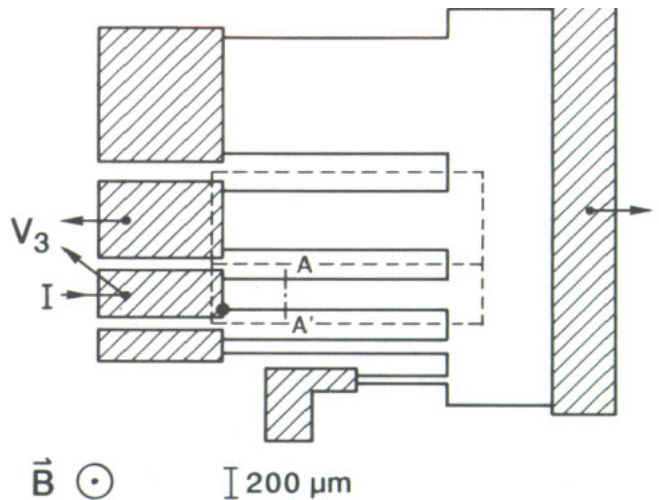


Figure 3. Lateral structure of the high-mobility zones. Alloyed contact areas are hatched. The path of the line profiles in figures 5 and 7 is marked between A and A'. Broken lines indicate the boundaries of the images shown in figures 6 and 8. The contact configuration for three-terminal measurements is also given. Note the location of the hot spot (black dot) for the indicated magnetic field direction.

where electron heating further increases the dissipative conductivity [14].

In samples with high mobility the longitudinal resistance near integral filling factors vanishes almost completely and more interesting effects than those of the above sample can be expected. A weakly doped heterostructure was prepared by molecular beam epitaxy which was optimized to avoid by-pass effects. On a semi-insulating (001) GaAs substrate of 0.5 mm thickness a $2.6 \mu\text{m}$ GaAs buffer was grown, followed by a 24 nm thick $\text{Al}_{0.33}\text{Ga}_{0.67}\text{As}$ spacer layer. A 55 nm layer with the same alloy composition and a volume doping of $3 \times 10^{17} \text{ cm}^{-3}$ Si followed and was in turn capped with 11 nm of GaAs. When this sample is cooled in the dark, no conductivity was measurable. Only upon exposure to ambient light through the window of the optical cryostat did a 2DES with density $3.7 \times 10^{11} \text{ cm}^{-2}$ and mobility $5.0 \times 10^5 \text{ cm}^2 \text{ V}^{-1} \text{ s}^{-1}$ persistently developed. This is consistent with a Fermi level pinned to the shallow donors in the doped region.

The probe wavelength of 850 nm is only 30 meV below the conduction band edge of GaAs at liquid-helium temperature; therefore residual absorption due to built-in vertical electric fields and impurities must be expected [16]. This will affect space charges and the lattice temperature to an unknown extent. With the present laser-scanning technique, however, this is, in the worst case, only a local perturbation which will not affect the overall potential landscape. There were no indications of parallel conduction (by-pass effects), or any other negative effects due to the laser irradiation in the samples presented here.

Using photolithography, a 2DES with the lateral structure depicted in figure 3 was defined. It resembles the shape of a hand with fingers of increasing width. This layout was initially designed to study the width

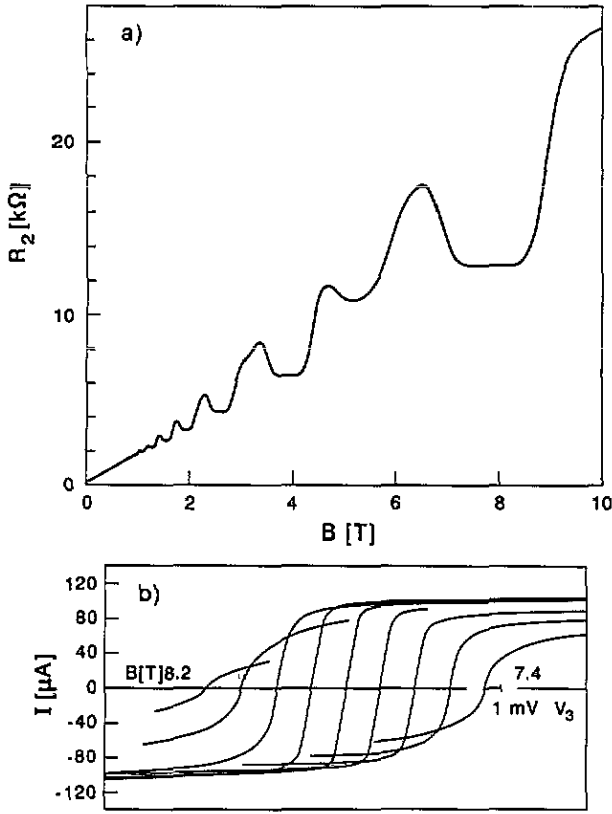


Figure 4. DC magnetotransport data used for sample characterization at $T = 1.5$ K. (a) Two-terminal resistance at $I = 10 \mu\text{A}$. (b) Three-terminal I - V characteristics around filling factor 2. The traces for various magnetic fields (incremented by 0.1 T) are shifted horizontally for clarity.

dependence of the QHE breakdown [17]. In the present work, the stripe of width $200 \mu\text{m}$ and length $1500 \mu\text{m}$ has been investigated. It is marked I for current injection. The boundaries of the details scanned are also indicated in figure 3. AuGe-Ni contacts (hatched areas) were alloyed to feed the transport current. On the polished rear face of the sample a 200 nm Au layer was evaporated onto 10 nm of Cr seed.

The two-terminal magnetoresistance of the high-mobility sample (figure 4(a), $I = 10 \mu\text{A}$) shows the pattern typical for high-quality samples. The longitudinal resistance is superimposed on the Hall resistance. It is well quantized around low-integer filling factors. Three-terminal I - V characteristics around filling factor 2 (figure 4(b), voltage contacts indicated by V_3 in figure 3) feature a pronounced breakdown behaviour, with a maximum critical current of $100 \mu\text{A}$ at $T = 1.6$ K. Towards the plateau edges, the I - V characteristics increasingly round off, as has been repeatedly observed [18, 19]. The finite slope of the I - V curves at zero bias in the plateau centre is due to the current lead resistance ($\approx 10 \Omega$); the resistance of the 2DES is much less than 1Ω at current values far below breakdown.

3. Experimental results

With the electro-optic method, images of the two-dimensional potential distributions set up by the respective transport currents were taken. Line profiles of the Hall potential (perpendicular to the current direction) were also scanned. All experiments were done around

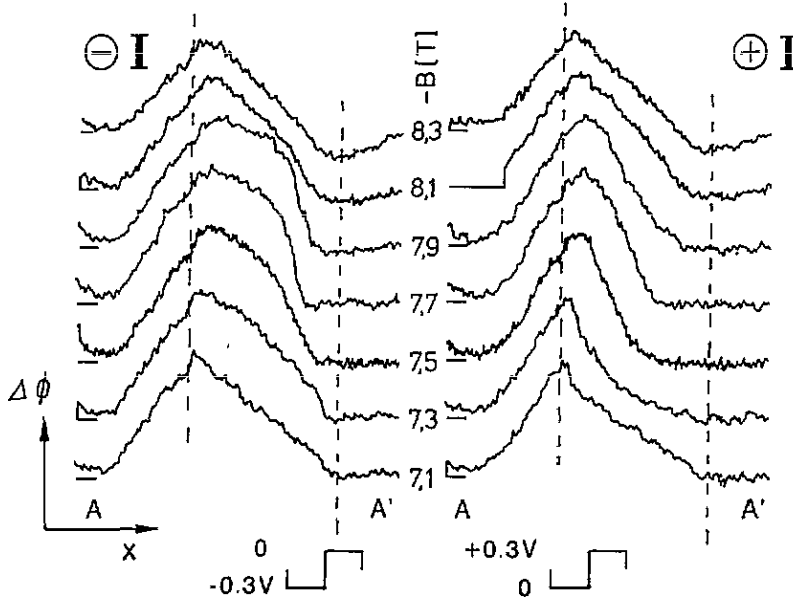


Figure 5. Hall potential profiles measured electro-optically across a $200 \mu\text{m}$ wide stripe, $400 \mu\text{m}$ from the source. The traces for various magnetic field values (central column) are shifted vertically for clarity. The value of the reference potential is given by the short horizontal line at the left side of each trace. In the left column the current is $-23 \mu\text{A}$, in the right column the polarity is reversed. The modulation scheme is symbolized at the bottom of the figure. Approximate positions of the edges (separated by $200 \mu\text{m}$) are indicated by broken vertical lines.

filling factor 2 at 1.6 K, with the sample immersed in superfluid helium.

3.1. Line profiles

Hall potential profiles taken along the line A–A' in figure 3, which is 400 μm from the source contact, are presented in figure 5. The transport current is switched on and off at a frequency of 320 Hz with a duty cycle of 50%. This is indicated at the bottom of the figure. The amplitude (peak to peak) of the two-terminal voltage of 0.3 V corresponds to a current value of 23 μA . The positions of the stripe edges are indicated with broken vertical lines. They were determined from a slight change in reflected light intensity and also independently from the increase in the signal fluctuations due to scattering at the etched edges of the minutely vibrating sample. The actual edge positions are uncertain within the diameter of the probe beam (15 μm). Zero electro-optical signal is indicated by the short horizontal line at the left of each trace. It corresponds to the potential of the reference electrode at the back of the sample.

Following a trace from right to left, the potential first fluctuates around zero. Within the channel, it then increases monotonically up to a maximum value. On the left, outside the channel, it decreases nearly to zero. There was no dependence on modulation frequency of the profiles inside the channel between 125 Hz and 10 kHz. This is different, however, in the bulk material between two neighbouring stripes, for example to the left of the left edge in figure 5. The edges of the neighbouring stripes are always at the same or nearly the same potential. In between one would expect from electrostatics that it drops to $0.8U_H$, U_H being the potential at the two adjacent stripes separated by 200 μm . Experimentally, we find that it varies from $0.1U_H$ at 125 Hz to $0.5U_H$ at 10 kHz. This frequency dependence is probably due to the combination of a geometrical capacitance (≈ 0.1 pF) and a charging resistance due to photogenerated carriers (≈ 100 M Ω) and is an effect of the bulk GaAs.

We now return to the potential profiles inside the channels. At a field just above the plateau ($B = -8.3$ T), the Hall potential profile is linear within the channel independent of polarity. This changes upon entering the QHR with decreasing magnetic field. Now the profiles deviate from linearity. In addition the evolution of the profile with magnetic field across the plateau is different for both current polarities. For negative current direction (left column), i.e. electrons flowing from left to right in figure 3, the Hall potential decrease mainly occurs in the right half of the channel. For positive current direction (right column), the behaviour is opposite: the Hall potential mainly drops in the left half of the stripe. The signals plotted have the same signs for both current polarities because we only inverted the DC bias to reverse polarity. This also facilitates comparison between the polarities. At the centre of the plateau ($B \approx -7.7$ T), the potential drop is steepest. Further decrease of the

magnetic field then yields a gradual transition towards the linear potential profile observed at the low-field side of the Hall plateau ($B \approx -7.1$ T).

At reversed magnetic field direction the potential profiles are reproduced within experimental error if the current polarity is simultaneously changed (not shown in the figure). No changes with the helium bath temperatures were observed from 1.2 K to 2.0 K.

3.2. Images

A series of images is compiled in figure 6 for three values of the magnetic field and both current directions. The boundaries of the 2DES stripe are indicated as black lines. At the left, the source contact is discernible. To the right, the stripe merges into the large 2DES area. The drain contact is outside the frame; the reference electrode at the backside is connected to the adjacent narrower finger outside the frame. The transport current modulation is 38 μA (peak to peak). The resulting two-terminal voltage is indicated at the left of the images. The evolution of the Hall potential profile in the middle of the stripe, which has already been discussed above, is reproduced (the colour code runs from green over yellow and red to violet for increasing potentials).

At a magnetic field just above the Hall plateau ($B = -8.3$ T), the potential drops linearly. Its slope is independent of polarity. It resembles the potential landscape expected from the conductivity model for a homogeneous system [1] and is similar to the one observed in the low-mobility sample. At the centre of the plateau, however, the profile is nonlinearly deformed ($B = -7.9$ T). The highest electric field occurs near the centre of the stripe, but its position is polarity dependent. This polarity dependence persists for lower magnetic fields ($B = -7.5$ T, still on the plateau). The maximal electric fields are, however, reduced in transition to the linear potential profile outside the QHR. The colour scales are equal for both current polarities because only the DC offset was changed to reverse the current direction, similar to the Hall profiles above.

In the images, there is a significant change of the potential profile at the two ends of the stripe. Close to the source, the potential distribution in the 2DES has to match that in the low-resistivity contact. However, the potential profile does not simply bend towards the current-injecting corner leading to the so-called hot spot: the potential drop becomes more linear in the transition region. Similarly, at the transition to the wider 2DES at the right, the Hall electric field reduces except in the plateau centre, where a steep potential drop persists into the wide region.

3.3. Nonlinear response

The observed nonlinear potential profiles depend on current magnitude as is demonstrated in figure 7 ($B = -7.7$ T, near the plateau centre). Hall potential profiles normalized to the respective current amplitudes are shown for both polarities. The respective two-terminal

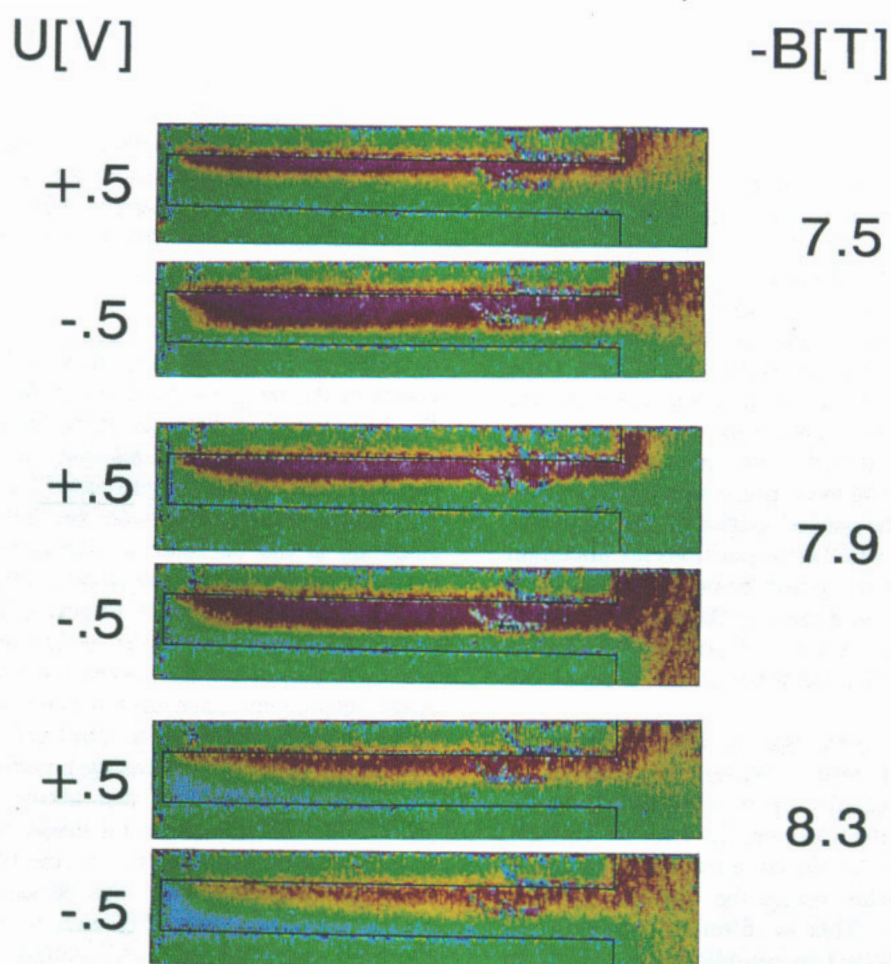


Figure 6. Electro-optic images of lateral potential distributions at three magnetic field values around filling factor 2. At each magnetic field (given in the right column) images for both polarities of the transport current are shown, with the Hall voltage indicated in the left column. The boundary of the 2DES is marked by the black line. The measured potential values are colour coded; they increase from green (= reference value) through yellow and red to violet.

voltages are given in the central column. The traces at ± 0.3 V have already appeared in figure 5 and are repeated here for completeness. The nonlinear behaviour of the profiles persists towards lower voltages. The polarity dependence, however, is gradually lost. The Hall potential profiles at $U = \pm 30$ mV (corresponding to $I = \pm 2.3$ μ A) are indistinguishable within the noise level.

For Hall voltages greater than 0.3 V the nonlinear potential profiles becomes increasingly rounded. For currents greater than the breakdown threshold ($I = 110$ μ A corresponding to $U = 1.5$ V), a linear potential profile is observed which is polarity independent. In analysing the experimental data, it must be taken into account that the probing beam diameter of approximately 15 μ m is not small compared to the extent of the observed features. So the maximum electric field at low current is possibly higher than that extracted from the traces.

The traces of figure 7 are normalized to the currents; thus the independence of the maximal electro-optic

signal from current shows that the electro-optic signal is proportional to the Hall voltage over nearly two orders of magnitude. This fact allows us to exclude additional potential drops at the edges of the 2DES at the lowest current. It also indicates that the 'chemical' part of the electrochemical potential discussed in the introduction can indeed be neglected. Distinct deviations are recognized only above the breakdown threshold, when dissipation introduces a longitudinal voltage drop. The observed maximum intensity modulation in each trace also agrees with the value estimated from the known electro-optic coefficient within at least 10%.

In summary, nonlinear potential profiles are always encountered in the QHR in our high-mobility sample. Current direction asymmetry, however, is only found for Hall voltages exceeding 0.2 V.

3.4. 'Non-local' effects

It is already apparent from figure 6 that the steep potential drop extends into the wide 2DES area at the

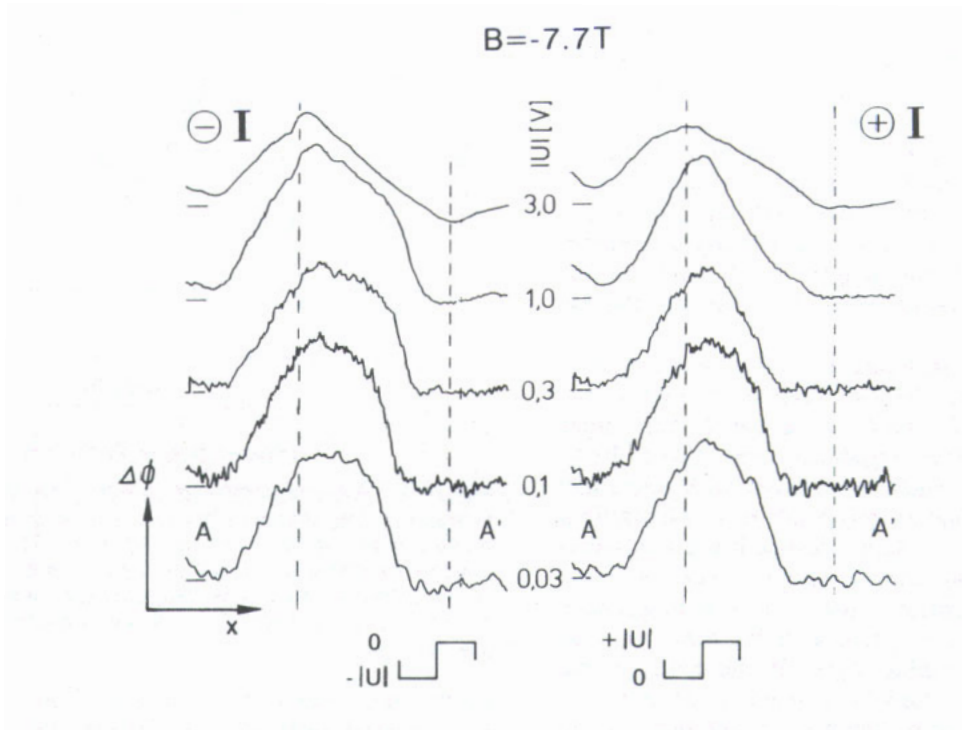


Figure 7. Hall voltage dependence of the electro-optically measured potential profiles at $B = -7.7$ T, $400 \mu\text{m}$ from the source. The amplitudes of the traces are normalized to the Hall voltage given in the central column. The right column is for positive current bias, the left column for negative bias according to the modulation scheme at the bottom of the figure. Again, the sample edges (separated by $200 \mu\text{m}$) are indicated by broken vertical lines and the reference potential values are marked by short horizontal lines.

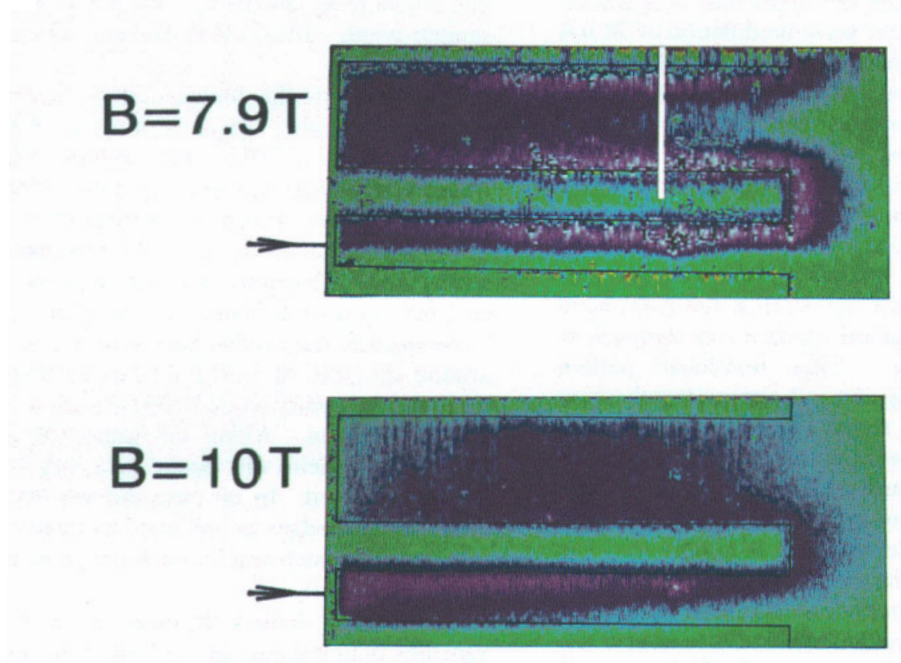


Figure 8. Electro-optic images of the potential distribution within a larger area of the sample. The upper image is taken in the α - π at filling factor 2, the lower one in the dissipative regime (filling factor ≈ 1.6). Boundaries of the 2DES are indicated by the black lines. The transport current enters the lower, narrow stripe via the source contact at the left edge. The measured potentials are colour coded; they increase from green (= reference value) through blue and violet to white.

right of the sample if the magnetic field is near the centre of the QHE plateau. This was studied further. Images of a larger area including the next widest stripe above are shown in figure 8. Two images are compared for magnetic fields on ($B = 7.9$ T) and off ($B = 10$ T) the Hall plateau. The edge of the 2DES is again indicated with black lines. Transport current is injected to the narrow stripe investigated previously. The stripe above is a 'dead end' of double width ($400 \mu\text{m}$), but equal length. It terminates in an alloyed contact discernible in the upper left of the images which is, however, unconnected. The drain electrode is on the right outside the frame.

The lower image in figure 8 is taken at a magnetic field of 10 T, where the two-terminal resistance has a value of $26.5 \text{ k}\Omega$ which is about $8 \text{ k}\Omega$ larger than the classical Hall resistance (see figure 4(a)). A symmetric square wave modulation with amplitude $33 \mu\text{A}$ is applied, which corresponds to a two-terminal voltage of ± 0.9 V. A large dissipative contribution clearly arises in the narrow stripe, where it leads to a potential distribution typical for a homogeneous conductor exposed to a magnetic field, similar to our results for the delta-doping layer. In the centre of the stripe, a Hall angle could be defined to describe the pattern assuming a homogeneous current distribution. At the same time, the upper, dead-end stripe is an equipotential area. This is also expected, since no current passes through it. The small inhomogeneities in the image are due to non-uniformities in the optical system.

In the QHR ($B = 7.9$ T), the potential distribution obviously looks different (see the upper part of figure 8). This time a symmetric square wave modulation of $38 \mu\text{A}$ (320 Hz) is applied, corresponding to a Hall voltage of ± 0.5 V. The behaviour in the narrow stripe has already been described above, although the polarity dependence is averaged out here. In the dead-end part there are even more drastic differences: it is no longer an equipotential area. Instead of that, the region of high Hall potential seems to follow the system edge, leaving a potential valley in the middle of the wider stripe. The penetration of the Hall potential at the right-hand side of the image is also greatly reduced in comparison with the dissipative case. This 'non-local' pattern disappeared with increasing currents approximately upon breakdown in the narrow stripe. At reversed magnetic field, analogous patterns were found.

The characteristic feature of the potential landscape in the QHR is quantified by a line scan across the wide stripe along the white line in figure 8 (figure 9). The approximate positions of the stripe edges are again given by the broken vertical lines. The potential across the wide stripe has a pronounced minimum ($\approx 0.3U_H$) in the middle; its value at the edges equals the Hall potential within the experimental error.

4. Analysis and discussion

We did not observe a frequency dependence of the potential profiles within 125 Hz and 10 kHz, thus we

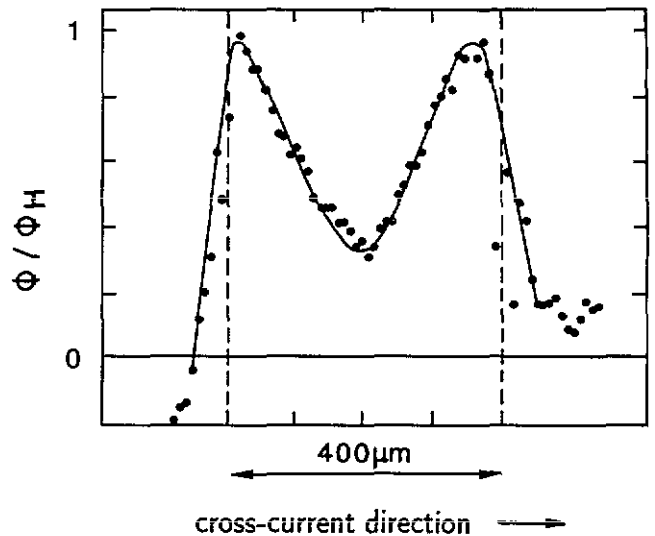


Figure 9. Potential profile taken along the white line in figure 8. The edges of the 2DES are indicated with broken vertical lines. In the QHR ($B = 7.9$ T), the stripe outside the classical current path (width $400 \mu\text{m}$) is not an equipotential area; it develops a pronounced potential minimum in the middle. The full line is meant as a guide to the eye.

confine ourselves to the stationary limit. Furthermore, the potential landscape is translationally invariant in current direction if we disregard the region near the contacts (figures 2 and 6).

In the delta-doping sample with low mobility we found linear potential profiles both inside and outside a QHE plateau. A linear profile is expected even in two dimensions if the current transport is dissipative and if the conductivity coefficients do not vary much over the sample width. This is a reasonable assumption for this sample.

By contrast, the high-mobility sample exhibited a step-like potential drop as long as the QHE effect was observed. This too agrees with the same phenomenological conductivity model if the assumption of homogeneous transport coefficients is dropped [20–23]. Such an inhomogeneity will originate from the very strong density dependence of the dissipative conductivity on both sides of a Shubnikov–de Haas minimum [24]. Consequently the current path will then be concentrated around the path of minimum conductivity (compatible with the boundary conditions) so as to minimize the total dissipation. Along the same path, the maximal Hall electric field will occur in a step-like fashion as indeed observed. In no case did we observe potential drops near the edges as predicted by quantum mechanical calculations which implied a homogeneously vanishing conductivity [10].

The strong density dependence of the conductivity vanishes both outside the QHE plateaus and for currents exceeding the value of breakdown of the QHE. The situation is now similar to the low-mobility sample. Indeed the observed potential distributions were linear across the high-mobility samples.

It has been postulated [21, 23] that electron density variations of the order of 1% are sufficient to explain the effect. Density variations of this order of magnitude may

be caused (i) by natural density inhomogeneities [2], (ii) by the Hall field itself via an electrostatic field effect with respect to a gate electrode and (iii) by photogeneration of carriers. The relative importance of these effects is discussed below.

The spatial resolution of our experiment ($10\ \mu\text{m}$) does not allow us to resolve inhomogeneities on the mesoscopic scale. Therefore it is not straightforward to discuss our results in terms of the edge-state model or in the one of the incompressible stripes. We now discuss the effects observed in the high-mobility sample under QHE conditions and discriminate them by the magnitude of the Hall voltage.

4.1. Linear response— $U_H < 0.2\ \text{V}$

The simplest way to produce a curved profile in linear response is the assumption of a density gradient perpendicular to the current direction. Due to the density dependence of conductivity, a potential profile with the steepest drop at the place of the minimum conductivity results [23]. Towards the plateau edges, the relative change of the conductivity with density is gradually reduced. This causes a gradual transition to a linear Hall potential profile outside the QHR, as we did indeed observe.

The reason for the density inhomogeneities postulated here is still to be explained. Inhomogeneities are doubtlessly already present across the original wafer, but their distribution should not be correlated with the lithographic structure, and their magnitude is probably lower than the 1% required for a sizable effect. Measurements with a Corbino disc geometry would clarify this point. Alternatively, it may also be possible that illumination by the infrared probe laser affects the carrier concentration although its wavelength is below the bandgap. The generation and or the recombination rates may be different near the edges of the sample leading to a sufficiently inhomogeneous carrier density distribution.

4.2. Nonlinear response— $U_H > 0.2\ \text{V}$

In our experiment, a transition to nonlinear response occurs at Hall voltages around $0.2\ \text{V}$. At this point the Hall voltage itself starts to influence the carrier concentration leading to the nonlinear response. A density variation of the order of 1% at a Hall voltage exceeding $0.2\ \text{V}$ is possible if there exists an effective gate electrode which is located $1\ \mu\text{m}$ away from the 2D plane. The only sensible length in this range is the buffer layer thickness. It is possible that a conductive layer forms at the substrate–buffer interface or that the Fermi energy is pinned at impurities at this interface. On the other hand, a screening electrode $1\ \mu\text{m}$ from the 2D plane has also been extracted previously [23] from an analysis of transport experiments on heterostructures with internal contacts in the dark [2]. The scenario of purely two-dimensional electrostatics without a gate, which has been analysed for the Corbino geometry [25], cannot account quantitatively for the observed

effect. For electric fields less than the breakdown value ($< 10^4\ \text{V m}^{-1}$) it always yields a linear potential profile.

An alternative explanation for the nonlinear response would again invoke photogenerated carriers drifting in the vertical field applied to the substrate by the 2DES and the reference electrode. These carriers could locally enhance or deplete the 2D density depending on the Hall voltage polarity. We believe, however, that this phenomenon would be restricted to the size of the probe beam, if it is relevant at all. From the longitudinal resistance measurement of the same 2DES in magnetic fields we conclude that the typical resistance between the 2DES and any parallel channels is greater than $100\ \text{M}\Omega$. Thus, the 2DES and the bulk material is electrically decoupled under average illumination. On the other hand, if there is a local disturbance at the probe beam due to the high local laser intensity it would have only a local effect and would not affect the overall potential landscape.

4.3. Breakdown behaviour and ‘non-local’ transport

Previous experiments on the breakdown of the QHE have been interpreted in terms of a critical current density at which dissipation starts to increase rapidly. A similar analysis has also been performed for the sample used here, yielding $j_c \approx 0.5\ \text{A m}^{-1}$ independent of channel width [17]. Above this critical current density, we observe a linear potential profile (see figure 7 at $U = \pm 3\ \text{V}$). The corresponding critical electric field $E_c \approx 6.5\ \text{kV m}^{-1}$ is equal, within experimental error, to the highest electric field within the channel at smaller currents, taken from figure 7 at $U_H = 1\ \text{V}$. At lower voltages this maximum electric field may possibly persist, but the corresponding potential slope would be too steep to be measured within our special resolution. Thus we suggest the following scenario compatible with the model of inhomogeneous transport coefficients: with increasing current the width of the region with electric field E_c increases until it reaches the sample width. Then the breakdown of the QHE as detected in standard transport experiments occurs.

Within this scenario a narrow stripe of maximal Hall field connects the two contacts at small currents. The observation of ‘non-local’ effects demonstrates that this line does not necessarily follow the geometrically shortest path as one would expect from classical electrostatics in dissipative media.

Steep decreases of the potential near the edges of the 2DES sample were observed in a previous electro-optic experiment [9]. In our experiment, however, a steep potential decrease near the centre of the sample was found. There exist, however, substantial differences between the experiments which are probably causing the conflicting results: first, the width of our sample is about 10 times less, $200\ \mu\text{m}$ as compared to $2\ \text{mm}$, which affects the time-scale required to reach diffusive equilibrium. Second, the wavelength of the probing light was $1300\ \text{nm}$ in [9] while it was $850\ \text{nm}$

in our experiment accentuating the possible effect of photogenerated carriers. Third, different intrinsic inhomogeneities must be expected in different samples.

In the QHR, the main potential drop has been found to occur within a narrow region due to the strong density dependence of the conductivity. Conceptually, this is an 'interior layer' similar to the well known boundary layer of classical fluid mechanics. There the major part of the velocity drop occurs close to the wall due to the small viscosity. Here, the important small parameter is the inverse logarithmic derivative of the conductivity with respect to the filling factor. In both cases a small parameter multiplies the leading derivative in the differential equation describing the transport process. The solution with prescribed boundary conditions features a layer-type behaviour. Problems of that type are called singularly perturbed in the mathematical literature [25]. In the QHR, there is still another kind of singular perturbation induced by the small conductivity, which is important for the dynamical response and results in 'non-local' potential patterns like figure 8. This may also be called a kind of 'skin effect'.

5. Conclusions

In conclusion, the linear electro-optic effect has been utilized to map transport-current-induced lateral potential distributions in magnetically quantized 2DES. Local subbandgap illumination in a scanning polarization microscope ensures minimal disturbance of the system. In a low-mobility sample ($\mu \approx 1.5 \times 10^3 \text{ cm}^2 \text{ V}^{-1} \text{ s}^{-1}$) we observed potential distributions as expected for a homogeneous system. In particular we found no inhomogeneities caused by the Hall potential itself.

In a high-mobility sample ($\mu \approx 5.0 \times 10^5 \text{ cm}^2 \text{ V}^{-1} \text{ s}^{-1}$) the observed potential distributions show: outside the QHR, the Hall potential drops linearly over the width of the stripe; inside the QHR, the potential profile is distinctly nonlinear with a pronounced maximum of the Hall electric field in the interior of the sample. This indicates current transport in the interior of the sample. Details of the potential profile depend continuously on filling factor and current value.

These nonlinear potential profiles are a consequence of a strong dependence of the transport coefficients on the carrier concentrations. Since the conductivity depends strongly on filling factor in the QHR, a pronounced bunching of the Hall potential drop will result. In our case both a carrier concentration gradient in the original sample and density inhomogeneities set up by the hall potential itself were necessary to explain all effects.

Effects related to edge channel or incompressible stripes near the edges were not necessary to describe the potential profiles. They will become important only on length scales much shorter than those available with the present technique. Even so, a rich spatial response

was encountered which reflects the quantum structure in the conductivity of the 2DES.

Acknowledgments

Contributions to this work by F Dietzel, A Fischer, U Klass, F Schartner and S Tippmann are gratefully acknowledged. One of us (RK) appreciates the introduction to electro-optics by J Kraus. This work was partly supported by the European Community.

References

- [1] Wakabayashi J and Kawaji S 1978 *J. Phys. Soc. Japan* **44** 1839
- [2] Ebert G, von Klitzing K and Weimann G 1985 *J. Phys. C: Solid State Phys.* **18** L257
Zheng H Z, Tsui D C and Chang A M 1985 *Phys. Rev. B* **32** 5506
Sichel E K, Sample H H and Salereno J P 1985 *Phys. Rev. B* **32** 6975
- [3] Haug R J 1993 *Semicond. Sci. Technol.* **8** 131
- [4] Ebert G, von Klitzing K, Ploog K and Weimann G 1983 *J. Phys. C: Solid State Phys.* **16** 5441
- [5] Chklovskii D B, Shklovskii B I and Glazman L I 1992 *Phys. Rev. B* **46** 4026
- [6] Iordanskii S V 1993 *JETP Lett.* **58** 316
- [7] Yariv A and Ye P 1984 *Optical Waves in Crystals* (New York: Wiley)
- [8] Wiesenfeld J M and Jain R K 1990 *Measurement of High Speed Signals in Solid State Devices (Semiconductors and Semimetals 28)* (Boston: Academic) p 221
- [9] Fontein P F, Hendriks P, Blom F A P, Wolter J H, Lochs H G M, Driessen F A J M, Giling L J and Beenakker C W J 1991 *Phys. Rev. B* **43** 12090
- [10] MacDonald A H, Rice T M and Brinkman W F 1983 *Phys. Rev. B* **28** 3648
- [11] Thouless D J 1985 *J. Phys. C: Solid State Phys.* **18** 6211
- [12] Knott R 1993 *PhD Thesis* Universität Stuttgart
- [13] Freeman J L, Jefferies S R and Auld B A 1987 *Opt. Lett.* **12** 795
- [14] Knott R, Dietsche W, von Klitzing K, Eberl K and Ploog K 1994 *Solid-State Electron.* **37** 689 (note that figure 2 in this publication was accidentally turned upside down)
- [15] Zrenner A, Koch F, Leotin J, Goiran M and Ploog K 1988 *Semicond. Sci. Technol.* **3** 1132
- [16] Weegels L M, Haverkort J E M, Leys M R and Wolter J H 1990 *Superlatt. Microstr.* **7** 315
- [17] Klass U 1992 *PhD Thesis* Universität Tübingen
- [18] Komiyama S, Takamasu T, Hiyamizu S and Sasa S 1985 *Solid State Commun.* **54** 479
- [19] Ahlers F J, Hein G, Scherer H, Bliek L, Nickel H, Lösch R and Schlapp W 1993 *Semicond. Sci. Technol.* **8** 2062
- [20] Pudalov V M and Semenchinskii S G 1985 *JETP Lett.* **42** 232
- [21] Woltjer R, Eppenga R, Mooren J and Timmering C E 1986 *Europhys. Lett.* **2** 149
- [22] Shashkin A A, Dolgoplov V T and Dorozhkin S I 1986 *Sov. Phys.-JETP* **64** 1124
- [23] Diener G and Collazo J 1988 *J. Phys. C: Solid State Phys.* **21** 3305
- [24] Tsui D C, Störmer H L and Gossard A C 1982 *Phys. Rev. B* **25** 1405
- [25] Smith D R 1985 *Singular-perturbation Theory* (Cambridge: Cambridge University Press)